



Nodal Space-Time Flux Reconstruction Methods for Conservation Laws

Meilin Yu¹ (✉)

Department of Mechanical Engineering
University of Maryland, Baltimore County (UMBC), Baltimore, MD 21250

A nodal space-time flux reconstruction (FR) method is developed to solve conservation laws. In this method, the spatiotemporal flow system is discretized in a finite-difference-like format without requirement for numerical quadrature. A dual time stepping method is used to solve the nonlinear system resulted from the space-time discretization. The nodal space-time FR method developed here can achieve arbitrarily high-order spatial and temporal accuracy without time step limitation. The numerical performance of this method has been verified with both the one dimensional (1D) and two dimensional (2D) linear wave propagation and nonlinear inviscid flow problems. It is found that if the Gauss-Legendre points are selected as solution points in the spatiotemporal element, the space-time FR method is superconvergent in time, no matter for the short- or long-term unsteady simulations. Similar to the findings reported by Asthana *et al.* (2017) [1], the space-time FR method shows superconvergent properties in space for long-term unsteady simulation.

I. Introduction

With the dramatic increase in computing power, computational fluid dynamics (CFD) has gradually become a very important method to explore challenging flow physics, e.g., those from atmospheric flow, turbomachinery flow, and bio-inspired flow. These flow physics usually feature unsteady multi-scale vortex structures over complex geometries. The discontinuous high-order methods on unstructured grids are promising candidates to accurately capture the multi-scale flow features over complex geometries. These methods include but not limited to discontinuous Galerkin (DG) [2, 3, 4, 5], staggered-grid multi domain (SGMD) [6, 7], spectral volume (SV) [8], spectral difference (SD) [9, 10], and flux reconstruction/correction procedure via reconstruction (FR/CPR) [11, 12, 13, 14].

We note that the high-order methods mentioned previously are mostly restricted to spatial discretization. The method-of-lines approach is usually adopted for time integration. If an explicit time marching method, e.g., the explicit Runge-Kutta method, is used to solve the semi-discretization form of the governing equations, the maximum time step is usually limited by the numerical stability requirement but not the flow physics. As a result, huge computational cost hinders the application of explicit time marching methods for practical flow simulation. Instead, implicit time marching methods, e.g., the backward differentiation formula (BDF), and the implicit Runge-Kutta method, can be used to improve the simulation efficiency. However, the BDF family with an order greater than two is not A-stable. Due to this deficiency, the second-order BDF is usually partnered with high-order spatial discretization to solve unsteady flow problems. Time steps should be small enough to ensure that temporal errors are consistent with those from spatial discretization. The implicit Runge-Kutta method can achieve higher-order of accuracy with good stability properties, but needs much effort to solve the resulting nonlinear system.

Alternatively, the space-time formulation provides a uniform treatment of both space and time [15]. Although some research [16, 17, 18] has been conducted for the space-time DG method, more work is still needed to fully explore the potential of this method. In this work, the nodal high-order space-time FR

¹ Assistant Professor, Department of Mechanical Engineering, AIAA Senior Member, email: mlyu@umbc.edu

method is developed. An implicit space-time method with right Radau points in time (equivalent to the Radau IIA method) has been developed by Huynh [19] for conservation laws. The FR approach is used in the derivation to reduce the weighted residual form to the differentiation one. Different from this approach, the time is treated as an extra dimension equivalent to the spatial dimension in the present study. Then a new space-time divergence term can be formulated. As a result, the FR approach can be used to directly reconstruct the space-time fluxes. As will be demonstrated later, the developed nodal space-time FR method can easily achieve arbitrarily high-order spatial and temporal discretization.

The remainder of the paper is organized as follows. In Section II, the nodal space-time FR method is introduced. Then dual time stepping methods to solve the space-time formulation are presented in Section III. The nodal space-time FR method is then tested with both the 1D and 2D linear advection problems and the nonlinear inviscid flow problems, and the results are reported in Section IV. Finally, Section V concludes the study.

II. Nodal space-time flux reconstruction method

Consider the conservation form of the compressible Euler equations,

$$\frac{\partial Q}{\partial t} + \nabla \cdot \mathbf{F}(Q) = 0, \quad (1)$$

defined on $\Omega \times [0, T]$ with the spatial domain Ω bounded by $\partial\Omega$, where Q is the vector of conserved variables, and \mathbf{F} is the spatial flux vector including both inviscid and viscous terms. Let $\mathbf{x} = (x_1, \dots, x_d)$ be the spatial coordinates, where the subscript ‘ d ’ stands for the dimension of the problem. Now we introduce the space-time domain $\Omega_{0 \rightarrow T}^{st} = \{(\mathbf{x}, t) | 0 \leq t \leq T, \mathbf{x} \in \Omega\}$, and the gradient operator $\nabla_{st} = (\partial_{x_1}, \partial_{x_2}, \dots, \partial_{x_d}, \partial_t)$ for the space-time domain. Eq. (1) can then be written as

$$\nabla_{st} \cdot \mathbf{F}^{st}(Q) = 0, \quad (2)$$

where $\mathbf{F}^{st}(Q) = (\mathbf{F}(Q), Q)$ is the space-time flux vector.

We approximate the exact solution using a space-time element-wise continuous polynomial $Q_h(\mathbf{x}, t) \in P^k(\Omega_{0 \rightarrow T}^{st})$, where P^k is the polynomial space of order equal to or less than k . Let $W(\mathbf{x}, t)$ be an arbitrary weighting function or test function. The weighted residual form of the governing equations on each space-time element $\Omega_{t_i \rightarrow t_{i+1}}^{st,j}$ (for simplicity, this is denoted as Ω_i^j) then reads

$$\int_{\Omega_i^j} \nabla_{st} \cdot \mathbf{F}^{st}(Q_h) W dV = 0. \quad (3)$$

Applying integration by parts twice to Eq. (3), one obtains

$$\int_{\Omega_i^j} \nabla_{st} \cdot \mathbf{F}^{st}(Q_h) W dV + \int_{\partial\Omega_i^j} (F_{com}^{st,n} - F^{st,n}) W dS = 0, \quad (4)$$

where $F^{st,n} = \mathbf{F}^{st} \cdot \mathbf{n}^{st}$. Note that to ensure conservation, the normal flux term $F^{st,n}$ from the first integration-by-parts operation is replaced with a common flux $F_{com}^{st,n}(Q_h^{i,j}, Q_h^{i+,j+}, \mathbf{n}^{st})$, where $Q_h^{i+,j+}$ denotes the solution outside the current element Ω_i^j , and \mathbf{n}^{st} is the outward unit normal vector of $\partial\Omega_i^j$. For the inviscid common flux (including Q in the space-time domain) calculation, various approximate Riemann solvers can be used, e.g. the Roe Riemann solver [20].

The surface integral in Eq. (4) is then cast into the form of a volume integral via the introduction of a correction field, i.e., $\delta^{st,C} \in P^k(\Omega_i^j)$. This is expressed as

$$\int_{\Omega_i^j} \delta^{st,C} W dV = \int_{\partial\Omega_i^j} (F_{com}^{st,n} - F^{st,n}) W dS. \quad (5)$$

On substituting Eq. (5) into Eq. (4), one obtains

$$\int_{\Omega_i^j} W (\nabla_{st} \cdot \mathbf{F}^{st}(Q_h) + \delta^{st,C}) dV = 0. \quad (6)$$

Denote a projection of $\nabla_{st} \cdot \mathbf{F}^{st}$ to $P^k(\Omega_i^j)$ by $\mathbb{P}(\nabla_{st} \cdot \mathbf{F}^{st})$. Then Eq. (6) can be reduced to a finite-difference-like format as

$$\mathbb{P}(\nabla_{st} \cdot \mathbf{F}^{st}) + \delta^{st,C} = 0. \quad (7)$$

This completes the derivation of the space-time FR formulation. For an efficient implementation, this formulation can be transformed into a standard (or computational) space-time element. In this study, Gauss-Legendre quadrature points are used in both the spatial and temporal discretization.

Compared with the method of lines using spatial FR/CPR discretization (this classical approach can be found in Ref. [21]), the space-time FR formulation Eq. (7) is intrinsically more compact and compute-bound. It can achieve arbitrarily high-order accuracy in both space and time with relatively small effort.

III. Dual time stepping methods

An efficient solution strategy for the nonlinear system (i.e., Eq. (7)) resulting from the new space-time formulation needs to be developed for excellent numerical performance. With the dual time stepping procedure, Eq. (7) is augmented with the pseudo-time derivative term as follows

$$\frac{\partial Q}{\partial \tilde{t}} + \mathbb{P}(\nabla_{st} \cdot \mathbf{F}^{st}(Q_h)) + \delta^{st,C} = \frac{\partial Q}{\partial \tilde{t}} + R^{st}(Q_h^n) = 0. \quad (8)$$

where \tilde{t} is the pseudo time, and the unsteady residual $R^{st} = \mathbb{P}(\nabla_{st} \cdot \mathbf{F}^{st}) + \delta^{st,C}$. A general practice is to directly solve this equation with the Newton's method [22]. In this approach, the nonlinear system is firstly linearized with respect to the current solution state Q_h^n . The resulting linear system becomes

$$\left(\frac{I}{\Delta \tilde{t}} + \left(\frac{\partial R^{st}}{\partial Q} \right)^n \right) \Delta Q = -R^{st}(Q_h^n), \quad (9)$$

where $\Delta Q = Q_h^{n+1} - Q_h^n$. We note that the size of the Jacobian matrix $\partial R^{st}/\partial Q$ can be very large, and the matrix pattern can be very complex for the unstructured mesh tessellated with space-time elements. To handle the memory and matrix pattern issues, the block LU-SGS method [23, 24, 25] can be used to solve the linearized space-time formulation. In this approach, instead of calculating the full Jacobian matrix $\partial R^{st}/\partial Q$, the elementwise Jacobian matrix $\partial R_c^{st}/\partial Q_c$, where the subscript 'c' stands for the current element, is calculated. Readers are referred to Ref. [26] for more details about the implementation of the block LU-SGS method in context of dual time stepping.

It is observed that the calculation of the elementwise Jacobian matrix $\partial R_c^{st}/\partial Q_c$ can still be very expensive for unsteady problems if it is computed during each physical time step. In this study, an explicit strong stability preserving (SSP) three-stage Runge-Kutta method is used for pseudo-time marching. This can be expressed as

$$\begin{cases} Q^{(1)} = Q^n + \Delta \tilde{t} R^{st}(Q^n) \\ Q^{(2)} = \frac{3}{4} Q^n + \frac{1}{4} Q^{(1)} + \frac{1}{4} \Delta \tilde{t} R^{st}(Q^{(1)}) \\ Q^{n+1} = \frac{1}{3} Q^n + \frac{2}{3} Q^{(2)} + \frac{2}{3} \Delta \tilde{t} R^{st}(Q^{(2)}) \end{cases}$$

We note that a similar explicit approach has been adopted in Ref. [16] to conduct pseudo-time stepping in a space-time DG method.

IV. Numerical results

In this section, the performance of the nodal space-time FR method is tested with the linear advection problems and the nonlinear inviscid flow problems. The L_2 errors of the numerical scheme are measured in two ways. In the first approach, the L_2 error is measured in the space-time slab $\Omega_n^{st} = \Omega \times [t_n - \Delta t, t_n]$ as

$$L_2(u; \Omega_n^{st}) = \left(\frac{\int_{\Omega_n^{st}} (u^\delta - u^{exact})^2 dV_{st}}{\int_{\Omega_n^{st}} 1 dV_{st}} \right)^{\frac{1}{2}}, \quad (10)$$

where u^δ is the numerical solution from the space-time FR method. In the second approach, the L_2 error is measured only in the spatial domain Ω at a specific time, e.g. the final time t_{final} of a simulation. This is written as

$$L_2(u; \Omega) = \left(\frac{\int_{\Omega} (u^{\delta,I} - u^{exact})^2 dV}{\int_{\Omega} 1 dV} \right)^{\frac{1}{2}}. \quad (11)$$

Herein, $u^{\delta,I}$ is the interpolated value from the space-time element. Specifically, $u_n^{\delta,I}$ can be calculated from the space-time slab $\Omega \times [t_n - \Delta t, t_n]$ as

$$u_n^{\delta,I} = \sum_{i=1}^N L_i(1) u_i^\delta, \quad L_i(\tau) = \prod_{j=1, j \neq i}^N \frac{\tau - \tau_j}{\tau_i - \tau_j}. \quad (12)$$

where $\tau_i \in [-1, 1]$, $i = 1, \dots, N$, are the temporal solution points in the standard space-time element.

IV.1. 1D linear advection problem

Consider the 1D linear wave equation,

$$\frac{\partial u}{\partial t} + \frac{\partial(cu)}{\partial x} = 0, \quad c > 0, \quad (13)$$

defined on the space-time domain $[0, 1] \times [0, +\infty)$. The initial condition is set as $u_0(x) = \sin(2\pi x)$, and $c = 1$ in this study.

The spatial convergence rates using P^1 to P^5 spatial reconstructions are shown in Figure 1. In Figure 1(a), the simulation is conducted until $t = 1$ (i.e., 1T). It is observed that the spatial convergence rates match the optimal values. In Figure 1(b), the histories of convergence rates for P^2 and P^3 spatial reconstructions are displayed during a long-term simulation. It is observed that the space-time FR schemes show superconvergent properties for long-term unsteady simulations. These observations agree with the discovery in Ref. [1].

The temporal convergence rates using P^1 to P^4 temporal reconstructions are presented in Figure 2. In Figure 2(a), the L_2 errors are calculated from the space-time slab $[1 - \Delta t, 1]$. The temporal convergence rates match the optimal values. In Figure 2(b), the L_2 errors are calculated at $t = 1$. It is clear that the temporal convergence rates show superconvergent properties. Specifically, for a P^k temporal reconstruction, the convergence rate is $2k + 1$. In Figure 2(c), the histories of convergence rates for P^2

and P^3 temporal reconstructions are displayed during a long-term simulation. It is found that the L_2 errors evaluated from the space-time slab $[t_n - \Delta t, t_n]$ show superconvergence during the entire simulation period; the L_2 errors evaluated at the time t_n gradually show superconvergence during the unsteady simulation, reaching $2k + 1$ for a P^k temporal reconstruction. The histories of the L_2 errors evaluated from the space-time slab $[t_n - \Delta t, t_n]$ and at the time t_n are displayed in Figure 3. It is found that the errors evaluated from the space-time slab will gradually approach those evaluated at the end time of the space-time slab.

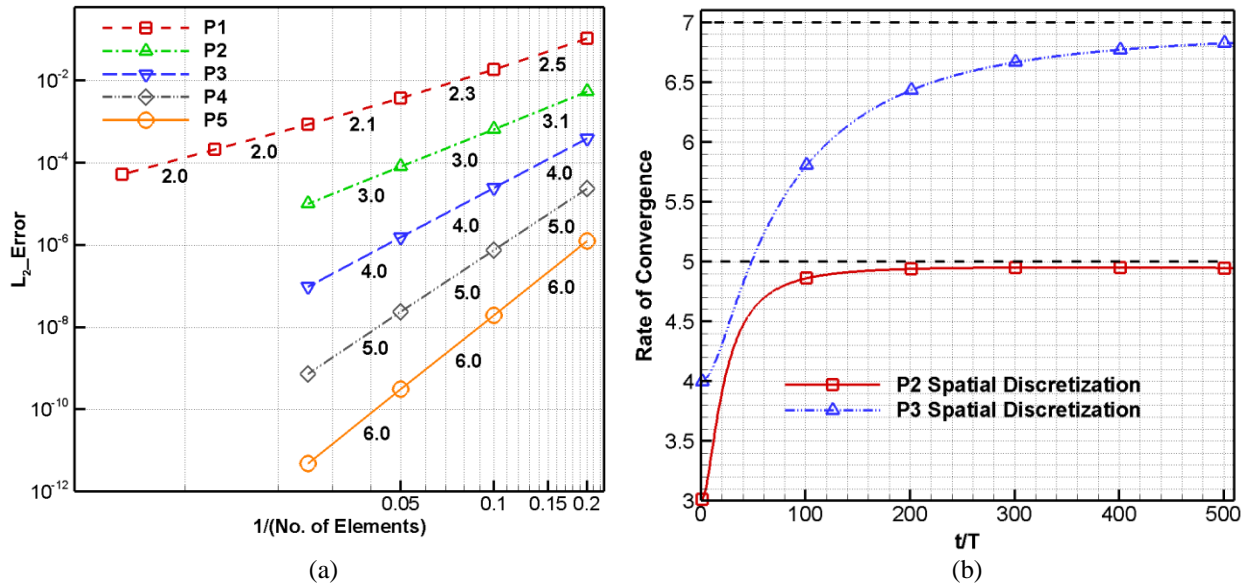
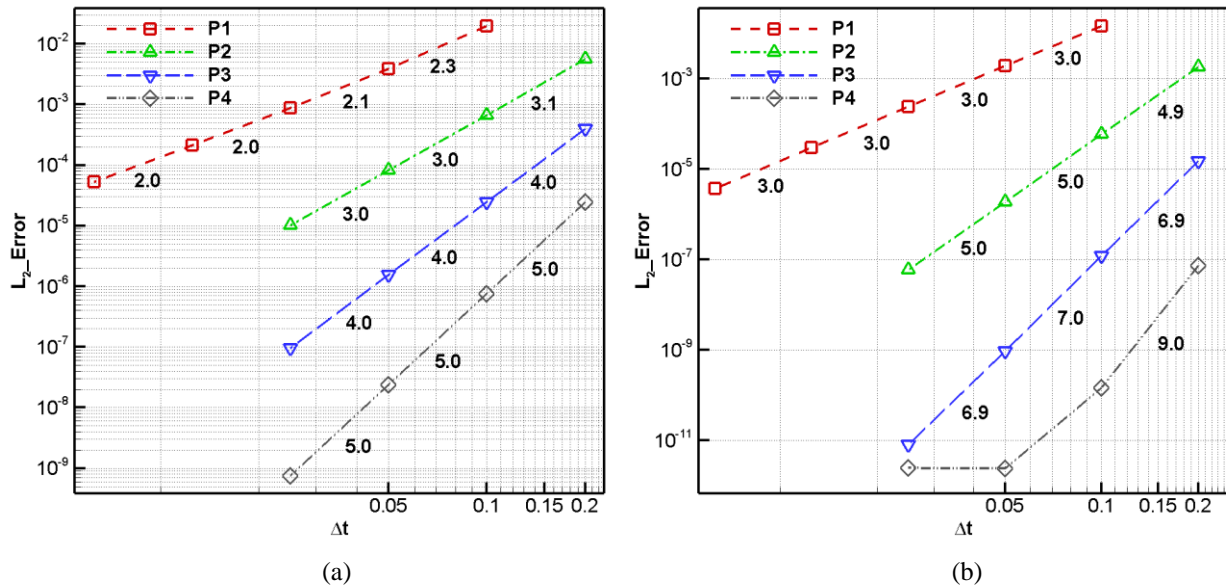


Figure 1. (a) Rates of spatial convergence from the grid refinement studies using P^1 to P^5 spatial reconstructions for the 1D linear wave equation at $t = 1$ (i.e. $1T$). (b) Long-term rates of convergence for P^2 and P^3 spatial reconstructions.



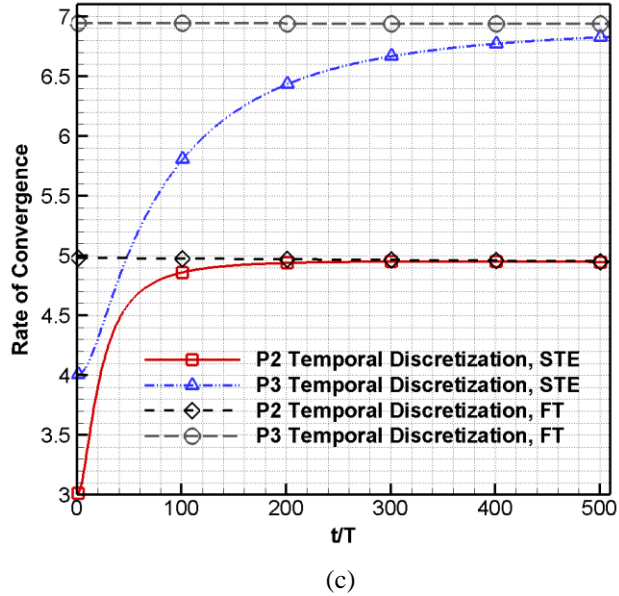


Figure 2. Rates of temporal convergence from the time-step refinement studies using P^1 to P^4 temporal reconstructions for the 1D linear wave equation at $t = 1$ (i.e. $1T$). (a) Rates of convergence evaluated from the last space-time slab $[1 - \Delta t, 1]$; and (b) rates of convergence evaluated at the final time $t = 1$. (c) Long-term rates of convergence evaluated from both the last space-time slab and the final time for P^2 and P^3 temporal reconstructions.

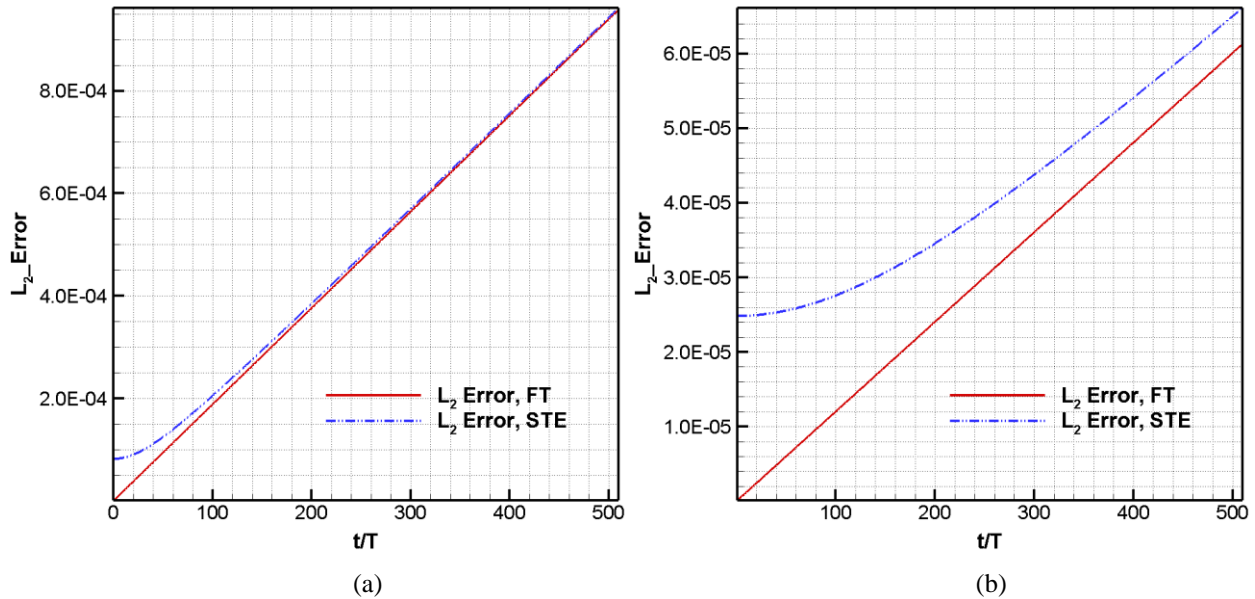


Figure 3. Histories of L_2 errors calculated at time t_n and from the corresponding space-time slab $[t_n - \Delta t, t_n]$. (a) L_2 errors of the P^2 temporal reconstruction; and (b) L_2 errors of the P^3 temporal reconstruction.

IV.2. Method of manufactured solutions for the Euler's equation with source terms

Consider the 1D Euler equation with source terms,

$$\frac{\partial Q}{\partial t} + \frac{\partial F}{\partial x} = S, \quad (14)$$

defined on the space-time domain $[-0.1, 0.2] \times [0, 0.5]$. Herein, the conservative variable and flux are expressed as

$$Q = \begin{pmatrix} \rho \\ \rho u \\ E_t \end{pmatrix}, F = \begin{pmatrix} \rho u \\ \rho u^2 + p \\ u(E_t + p) \end{pmatrix},$$

where ρ is the fluid density, u is the velocity, p is the pressure, and E_t is the total energy expressed as

$$E_t = \frac{p}{\gamma - 1} + \frac{1}{2} \rho u^2.$$

In the method of manufactured solutions (MMS), the source terms are calculated from the exact solution

$$\begin{cases} \rho = 0.5(\sin(x^2 + t^2) + 1.5) \\ u = \sin(x^2 + t^2) + 0.5 \\ E_t = 0.5(\cos(x^2 + t^2) + 1.5) \end{cases}. \quad (15)$$

Similar to the linear advection problem, the L_2 errors are measured both from the space-time slab $\Omega_n^{st} = \Omega \times [t_{final} - \Delta t, t_{final}]$ and at the final time.

The spatial convergence rates for the space-time FR schemes using P^1 to P^5 spatial reconstructions are presented in Figure 4(a). In this case, the Rusanov Riemann solver is used. From the grid refinement study, the convergence rates of the even orders (i.e. P^1 , P^3 , and P^5) can reach the optimal values. The convergence for the odd order (i.e. P^2 , and P^4) is slow but its rate approaches the optimal value when the grid size decreases. The temporal convergence rates evaluated from the last space-time slab $[0.5 - \Delta t, 0.5]$ and at the final time $t = 0.5$ using P^1 to P^4 temporal reconstructions are presented in Figure 4(b) and 4(c), respectively. The temporal convergence rates evaluated from the space-time slab reach the optimal value. Due to the source terms, the L_2 errors calculated at the final time do not show apparent superconvergent features.

The spectral convergence properties are also tested for this problem. The results for the spatial spectral convergence tests are presented in Figure 5(a) and those for the temporal spectral convergence tests are presented in Figure 5(b). It is clear that both spatial and temporal discretization has shown the spectral convergence properties.

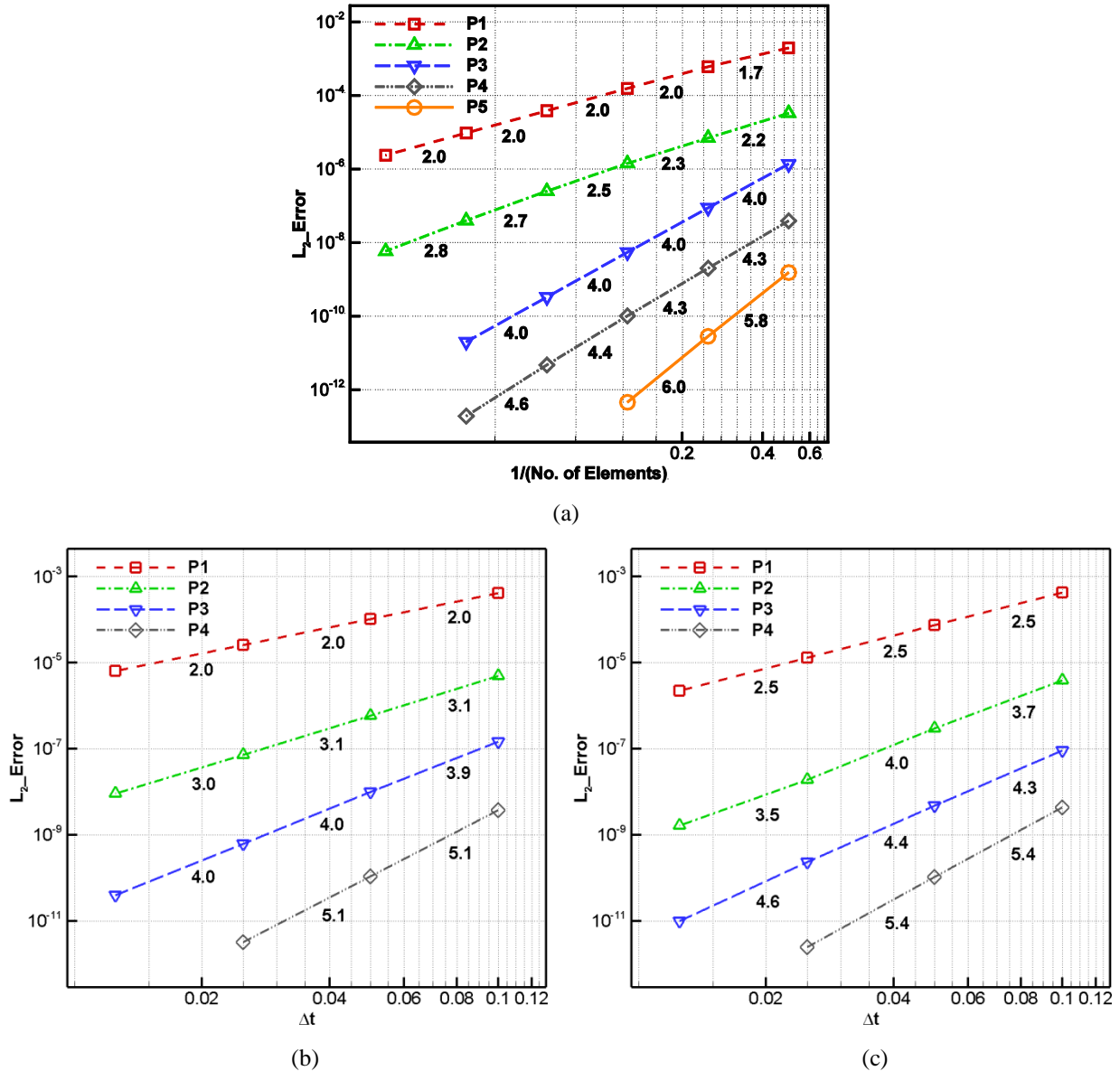


Figure 4. (a) Rates of spatial convergence from the grid refinement studies using P^1 to P^5 spatial reconstructions for the 1D MMS at $t = 0.5$; (b) rates of temporal convergence evaluated from the last space-time slab $[0.5 - \Delta t, 0.5]$ using P^1 to P^4 temporal reconstructions; and (c) rates of temporal convergence evaluated at the final time $t = 0.5$ using P^1 to P^4 temporal reconstructions.

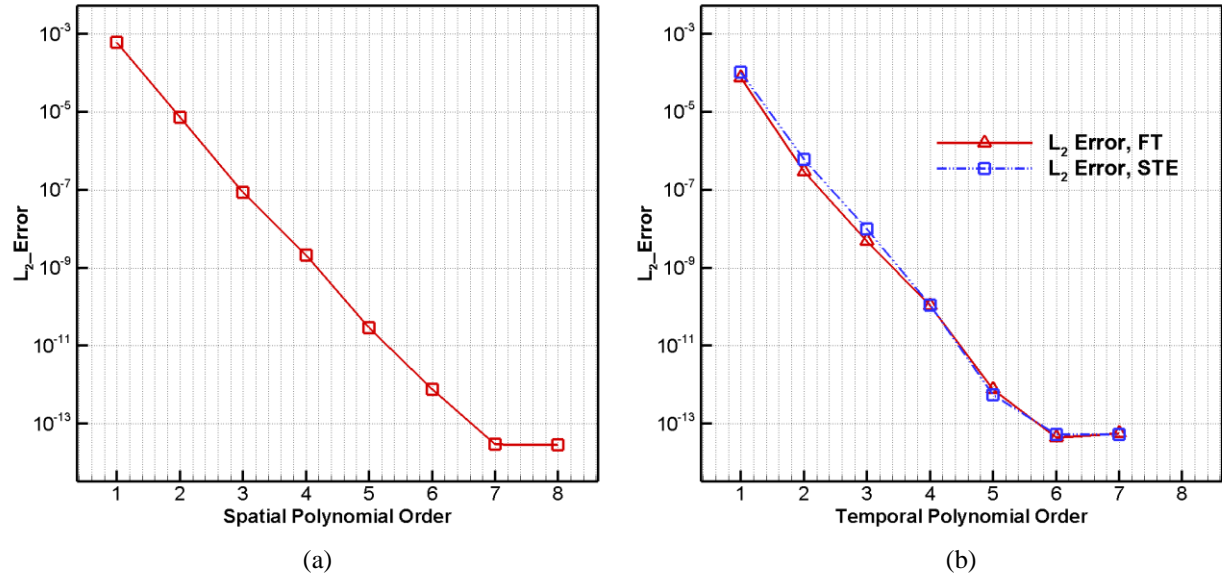


Figure 5. (a) Spatial and (b) temporal spectral convergence tests for the 1D MMS. Note that in (b) the L_2 errors are evaluated both at the final time $t = 0.5$ and from the last space-time slab $[0.5 - \Delta t, 0.5]$.

IV.3. 2D linear advection problem

Consider the 2D wave equation,

$$\frac{\partial u}{\partial t} + \frac{\partial(c_1 u)}{\partial x} + \frac{\partial(c_2 u)}{\partial y} = 0, \quad (16)$$

where c_1 and c_2 are the wave speeds in the x - and y -directions, respectively. In this study, $c_1 = 0.5$ and $c_2 = 0.5$. The computational domain is $[-2, 2] \times [-2, 2]$.

The spatial convergence rates using P^1 to P^5 spatial reconstructions, and the temporal convergence rates evaluated at the final time $t = 4$ (i.e. 1T) using P^1 to P^3 temporal reconstructions are presented in Figures 6(a) and 6(b), respectively. From the grid refinement study, it is observed that the spatial convergence rates match the optimal values. For the temporal convergence study, the L_2 errors from P^1 to P^3 temporal reconstructions are calculated at the final time. It is observed that the temporal convergence rates show superconvergent features. Specifically, for a P^k temporal reconstruction, the convergence rate is $2k + 1$.

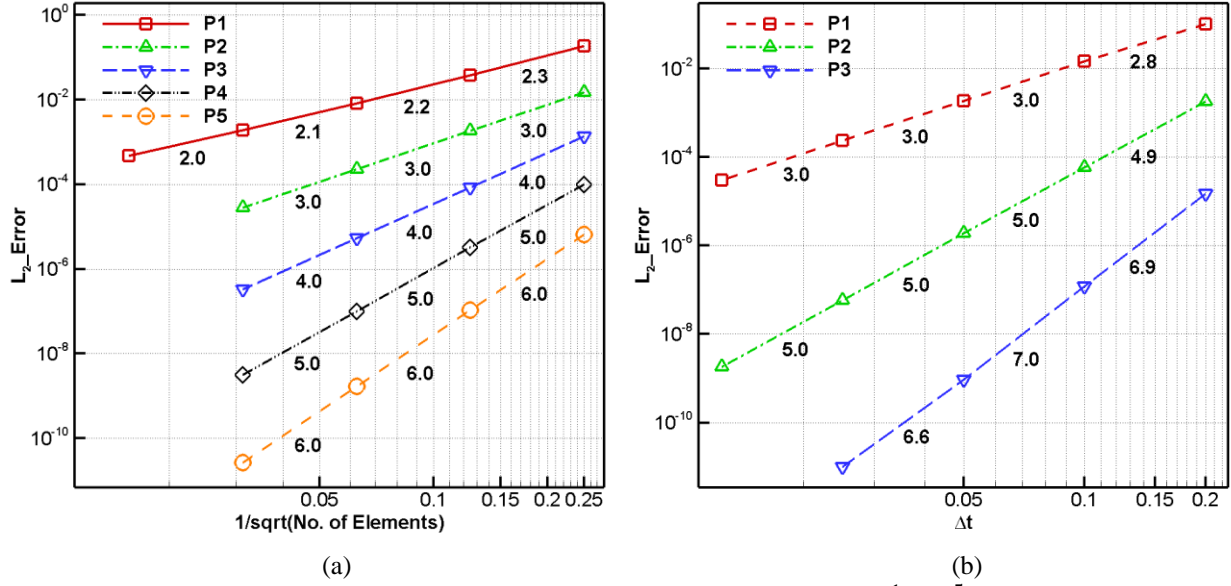


Figure 6. (a) Rates of spatial convergence from the grid refinement studies using P^1 to P^5 spatial reconstructions for the 2D advection problem at $t = 4$ (i.e. 1T); and (b) rates of temporal convergence evaluated at the final time $t = 4$ using P^1 to P^4 temporal reconstructions.

IV.4. 2D isentropic vortex propagation

The 2D Euler equation can be written as

$$\frac{\partial Q}{\partial t} + \frac{\partial F}{\partial x} + \frac{\partial G}{\partial y} = 0, \quad (17)$$

where the conservative variable and fluxes are expressed as

$$Q = \begin{pmatrix} \rho \\ \rho u \\ \rho v \\ E_t \end{pmatrix}, F = \begin{pmatrix} \rho u \\ \rho u^2 + p \\ \rho uv \\ u(E_t + p) \end{pmatrix}, G = \begin{pmatrix} \rho v \\ \rho uv \\ \rho v^2 + p \\ v(E_t + p) \end{pmatrix}.$$

Following Ref. [27], one analytical solution for the isentropic vortex can be given as

$$\begin{cases} \rho = \left(1 - \frac{1}{2}(\gamma - 1)u_{max}^2 e^{1 - \frac{r^2}{b^2}}\right)^{1/(\gamma-1)} \\ p = \frac{1}{\gamma} \left(1 - \frac{1}{2}(\gamma - 1)u_{max}^2 e^{1 - \frac{r^2}{b^2}}\right)^{\gamma/(\gamma-1)} \\ u = U_0 - \frac{u_{max}}{b} r e^{\frac{1}{2}\left(1 - \frac{r^2}{b^2}\right)} \sin\theta \\ v = V_0 + \frac{u_{max}}{b} r e^{\frac{1}{2}\left(1 - \frac{r^2}{b^2}\right)} \cos\theta \end{cases}.$$

Herein, $r = \sqrt{(x - U_0 t)^2 + (y - V_0 t)^2}$, U_0 and V_0 are the advection velocities of the free stream in the x - and y -directions, respectively, and θ is the angle with respect to the x -direction. In this study, $(U_0, V_0) = (0.5, 0)$, $u_{max} = 0.25$, and $b = 0.2$. The computational domain is $[-2, 2] \times [-2, 2]$.

The spatial convergence rates using P^2 to P^5 spatial reconstructions at $t = 0.5$ (i.e. $T/8$) are displayed in Figure 7. In this case, the Roe Riemann solver is used. From the grid refinement study, the spatial convergence rates can reach the optimal values. For the temporal convergence study, the L_2 errors are evaluated at $t = 4$ (i.e. $1T$) and from the space-time slab $[4 - \Delta t, 4]$. The results are presented in Figure 8. It is observed that when the L_2 errors are calculated at $t = 4$, the temporal convergence rates can reach $2k + 1$ for a P^k temporal reconstruction; when the L_2 errors are calculated from the space-time slab $[4 - \Delta t, 4]$, the temporal convergence rates match the optimal values.

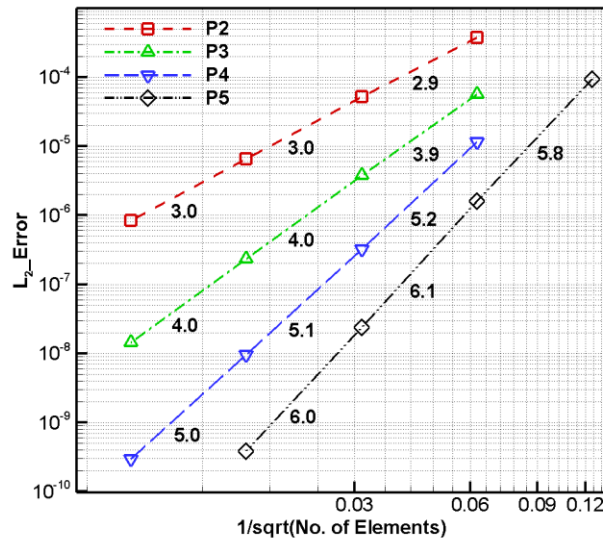


Figure 7. Rates of spatial convergence from the grid refinement studies using P^2 to P^5 spatial reconstructions for the 2D isentropic vortex propagation at $t = 0.5$ (i.e. $T/8$).

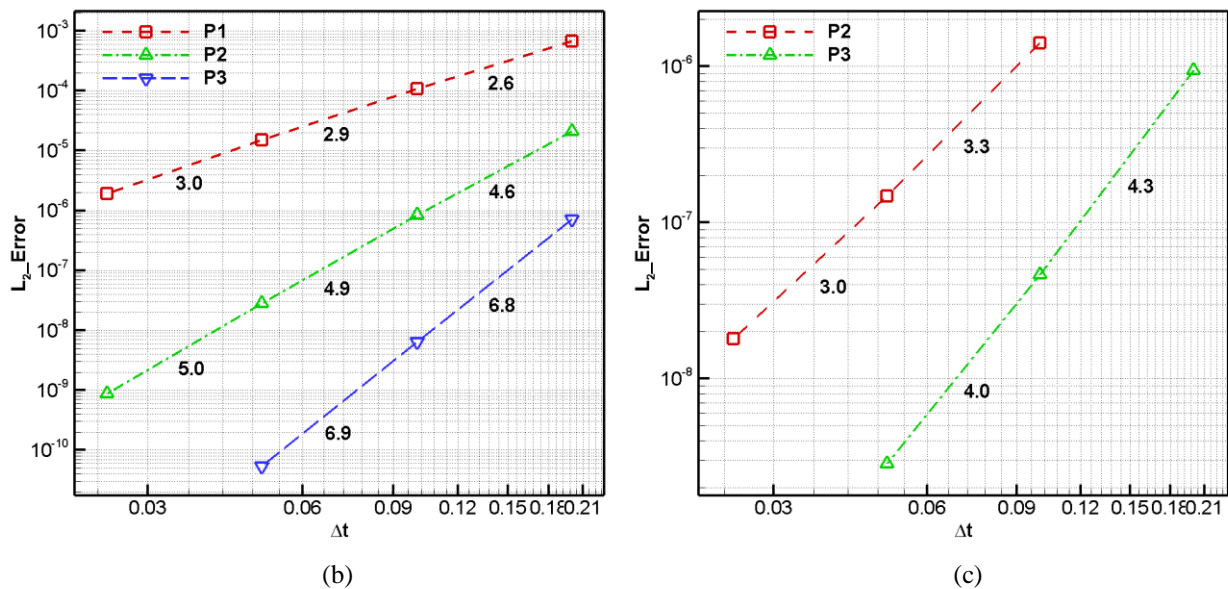


Figure 8. (a) Rates of temporal convergence evaluated at the final time $t = 4$ (i.e. $1T$) using P^1 to P^3 temporal reconstructions; and (b) rates of temporal convergence evaluated from the last space-time slab $[4 - \Delta t, 4]$ using P^2 and P^3 temporal reconstructions.

V. Conclusions

In this study, a nodal space-time FR method is developed to solve conservation laws. A dual time stepping strategy with the explicit SSP Runge-Kutta method is used to march the nonlinear system originated from the space-time discretization in pseudo time. The space-time formulation is in the differentiation form with no numerical quadrature involved in calculation. This formulation can easily achieve arbitrarily high-order spatial and temporal accuracy. Both 1D and 2D linear wave propagation and nonlinear inviscid flow problems are simulated to verify its numerical performance. Several observations are summarized as follows:

- For hyperbolic equations without source terms, the space-time FR method using Gauss-Legendre points is spatially superconvergent during long-term unsteady simulations. Specifically, for a P^k spatial reconstruction, the convergence rate of the numerical scheme is $2k + 1$. This has been reported by Asthana *et al.* (2017) for the FR method in a semi-discretization form.
- When the errors are measured from the space-time slab, for hyperbolic equations without source terms, the space-time FR method using Gauss-Legendre points is temporally superconvergent during long-term unsteady simulations. Specifically, for a P^k temporal reconstruction, the convergence rate of the numerical scheme is $2k + 1$. For short-term simulation, the temporal convergence rates match the optimal values.
- When the errors are measured at any specific time, for hyperbolic equations without source terms, the space-time FR method using Gauss-Legendre points is temporally superconvergent during both short-term and long-term unsteady simulations. However, if there exist source terms in the governing equations, the superconvergent features do not strictly hold. More study is still needed to examine the numerical properties of the space-time FR method.

Acknowledgement

The author gratefully acknowledges the support of the Office of Naval Research through the award N00014-16-1-2735, and the faculty startup support from the department of mechanical engineering at University of Maryland, Baltimore County (UMBC).

References

- [1] K. Asthana, J. Watkins and A. Jameson, "On consistency and rate of convergence of Flux Reconstruction for time-dependent problems," *Journal of Computational Physics*, vol. 334, pp. 367-391, 2017.
- [2] B. Cockburn and C.-W. Shu, "TVB Runge-Kutta local projection discontinuous Galerkin finite element method for conservation laws II: general framework," *Mathematics of Computation*, vol. 52, pp. 411-435, 1989.
- [3] F. Bassi and S. Rebay, "A high-order accurate discontinuous finite element method for the numerical solution of the compressible Navier-Stokes equations," *J. Comput. Phys.*, vol. 138, pp. 251-185, 1997.
- [4] J. S. Hesthaven and T. Warburton, *Nodal discontinuous Galerkin methods – algorithms, analysis and applications*, New York: Springer, 2008.
- [5] J. Peraire and P.-O. Persson, "High-order discontinuous Galerkin methods for CFD," in *Adaptive High-Order Methods in Computational Fluid Dynamics*, Z. J. Wang, Ed., World Scientific Series in

Advances in Computational Fluid Dynamics, 2011, pp. 119-152.

- [6] D. A. Kopriva and J. H. Kalias, "A conservative staggered-grid Chebyshev multidomain method for compressible flows," *J. Comput. Phys.*, vol. 125, pp. 244-261, 1996.
- [7] D. A. Kopriva, "A staggered-grid multidomain spectral method for the compressible Navier–Stokes equations," *J. Comput. Phys.*, vol. 143, pp. 125-158, 1998.
- [8] Z. J. Wang, "Spectral (finite) volume method for conservation laws on unstructured grids: basic formulation," *J. Comput. Phys.*, vol. 178, pp. 210-251, 2002.
- [9] Y. Liu, M. Vinokur and Z. J. Wang, "Spectral difference method for unstructured grids I: Basic formulation," *J. Comput. Phys.*, vol. 216, pp. 780-801, 2006.
- [10] Z. J. Wang, Y. Liu, G. May and A. Jameson, "Spectral difference method for unstructured grids II: extension to the Euler equations," *J. Sci. Comput.*, vol. 32, pp. 45-71, 2007.
- [11] H. T. Huynh, "A flux reconstruction approach to high-order schemes including discontinuous Galerkin methods," in *the 18th AIAA Computational Fluid Dynamics Conference*, Miami, FL, 2007.
- [12] H. T. Huynh, "A reconstruction approach to high-order schemes including discontinuous Galerkin for diffusion," in *the 47th AIAA Aerospace Sciences Meeting Including The New Horizons Forum and Aerospace Exposition, AIAA 2009-403*, Orlando, FL, 2009.
- [13] Z. J. Wang and H. Y. Gao, "A unifying lifting collocation penalty formulation including the discontinuous Galerkin, spectral volume/difference methods for conservation laws on mixed grids," *Journal of Computational Physics*, vol. 228, pp. 8161-8186, 2009.
- [14] P. E. Vincent, P. Castonguay and A. Jameson, "A new class of high-order energy stable flux reconstruction schemes," *J. Sci. Comput.*, vol. 47, no. 1, pp. 50-72, 2011.
- [15] L. M. Wang and P.-O. Persson, "A high-order discontinuous Galerkin method with unstructured space-time meshes for two-dimensional compressible flows on domains with large deformations," *Comput. & Fluids*, vol. 118, pp. 53-68, 2015.
- [16] J. van der Vegt and H. van der Ven, "Space–Time Discontinuous Galerkin Finite Element Method with Dynamic Grid Motion for Inviscid Compressible Flows: I. General Formulation," *Journal of Computational Physics*, vol. 182, pp. 546-585, 2002.
- [17] S. Petersen, C. Farhat and R. Tezaur, "A space-time discontinuous Galerkin method for the solution of the wave equation in the time-domain," *Int. J. Numer. Meth. Engng*, vol. 78, pp. 275-295, 2009.
- [18] M. Feistauer and J. Česenek, "Space-time discontinuous Galerkin finite element method for convection-diffusion problems and compressible flow," in *Numerical methods and applications*, I. Dimov, S. Dimova and N. Kolkovska, Eds., Berlin, Springer, 2011, pp. 1-13.
- [19] H. T. Huynh, "High-order space-time methods for conservation laws," in *21st AIAA Computational Fluid Dynamics Conference, 2013-2432*, San Diego, CA, 2013.
- [20] P. L. Roe, "Approximate Riemann solvers, parameter vectors and difference schemes," *J. Comput. Phys.*, vol. 43, no. 2, pp. 357-372, 1981.
- [21] M. L. Yu, Z. J. Wang and Y. Liu, "On the accuracy and efficiency of discontinuous Galerkin, spectral difference and correction procedure via reconstruction methods," *Journal of Computational*

Physics, vol. 259, pp. 70-95, 2014.

- [22] P.-O. Persson and J. Peraire, "Newton-GMRES preconditioning for discontinuous Galerkin discretizations of the Navier-Stokes equations," *SIAM J. Sci. Comput.*, vol. 30, pp. 2709-2733, 2008.
- [23] S. Yoon and A. Jameson, "Lower-upper symmetric-Gauss-Seidel method for the Euler and Navier-Stokes equations," *AIAA Journal*, vol. 26, pp. 1025-1026, 1988.
- [24] Y. Z. Sun, Z. J. Wang and Y. Liu, "Efficient implicit non-linear LU-SGS approach for compressible flow computation using high-order spectral difference method," *Communication of Computational Physics*, vol. 5, pp. 760-778, 2009.
- [25] M. L. Yu, Z. J. Wang and H. Hu, "A high-order spectral difference method for unstructured dynamic grids," *Computers & Fluids*, vol. 48, pp. 84-97, 2011.
- [26] M. L. Yu and L. Wang, "A high-order flux reconstruction/correction procedure via reconstruction formulation for unsteady incompressible flow on unstructured moving grids," *Computers & Fluids*, vol. 139, pp. 161-173, 2016.
- [27] F. Q. Hu, X. D. Li and D. K. Lin, "Absorbing boundary conditions for nonlinear Euler and Navier-Stokes equations based on the perfectly matched layer technique," *Journal of Computational Physics*, vol. 227, pp. 4398-4424, 2008.